Premio SOCIEMAT Mejor Trabajo de Fin de Máster en Ingeniería en Materiales 2023

ORGANIC FIELD-EFFECT TRANSISTORS FOR NEAR-INFRARED LIGHT DETECTION

***L. Casabona-Cendra*[1], *C. Martínez-Domingo*[1], *S. Riera-Galindo*[1], *M. Campoy-Quiles*[1], *M. Mas-Torrent*[1]**

[1]Institute of Materials Science of Barcelona, Campus UAB, 08193, Bellaterra, Spain, lcasabona@icmab.es

Abstract: Organic photodetectors (OPDs) have recently attracted continuous attention owing to the remarkable advantages offered by organic semiconductors (OSCs) with respect to their inorganic counterparts, including low-cost processability, lightweight, semitransparency, good absorption coefficient and the ability to be chemically tuned. Among these, near-infrared (NIR) OPDs hold particular significance given their potential applications in areas such as health-monitoring, night vision, and optical communications. However, developing new OSCs with suitable properties for NIR light detection remains a challenge. In this work, the properties of the non-fullerene acceptor (NFA) molecule Y6 have been studied in organic phototransistors (OPTs) based on organic field-effect transistors (OFETs) fabricated using low-cost techniques. The devices have been characterized by X-ray diffraction (XRD) and polarized optical microscopy (POM). Furthermore, the photoresponse of the OSC has been explored by conducting electrical measurements on the devices, both with and without incident radiation.

Keywords: Y6, non-fullerene acceptors, organic semiconductors, organic field-effect transistors, near-infrared sensors.

1. INTRODUCTION.

Near-infrared (NIR) light detection plays an important role in modern science and technology, such as in health monitoring, night vision, artificial vision, optical communications, and spectroscopy, among others [1]. Current NIR photodetectors predominantly rely on photodiodes based on inorganic semiconductors such as silicon (Si), germanium (Ge), and other III to V compounds. However, these devices often present some drawbacks, such as high brittleness, complicated and not environmentally friendly manufacturing processes, and broadband absorption. In the last decades, solution-processed NIR-sensitive organic semiconductors (OSCs), which can be highly conjugated small organic molecules or polymers, have emerged as attractive alternatives to their inorganic counterparts, due mainly to their low cost processability, tailorable optoelectronic properties, and compatibility with flexible substrates [2].

Devices based on OSCs that can convert light into electrical signals are commonly referred to as organic photodetectors (OPDs). OPDs can be categorized into three main types: organic photodiodes, photoconductors, and phototransistors (OPTs). OPTs can be built on organic field-effect transistors (OFETs), which are three-terminal devices where the current flow from two of them (source (S) and drain (D)) can be modulated by the application of a voltage in the third electrode (gate (G)). In OFETs, an ordered structure (high crystallinity) of the OSC is highly desirable as it reduces the density of traps in the conductive channel and therefore increases the current flow in the OSC, improving the electrical performance of the devices. OFETs can have different architectures depending on the relative position of the electrodes with respect to the OSC. A schematic representation of an OFET with a bottom-gate bottom-contact (BGBC) architecture is depicted in **Fig. 1a**.

One of the greatest challenges for NIR OPDs is to design and synthesize organic photoactive materials with ultra-narrow bandgaps. One approach to tackle this is extending the conjugation length of polymers. However, polymer's intrinsic drawbacks such as large structure disorder can limit the performance of polymer based NIR OPDs. On the other hand, small-molecule semiconductors with well-defined structures and with acceptor-donor-acceptor (A-D-A) designs have arisen as promising candidates for high-sensitivity OPDs [3]. One promising candidate to address this challenge is Y6, a non-fullerene acceptor (NFA) semiconductor with an A-DA'D-A structure as illustrated in **Fig. 1b**, where grey and blue areas represent the A segments of Y6 while yellow represent the D segments. This relatively new organic material was first developed by Zou and co-workers in 2019 [4] and has been extensively investigated for high-performance organic solar cells. Y6 has shown interesting optoelectronic properties such as high charge mobility for an n-type OSC [5] and capacity to absorb light within a specific region of the NIR spectrum, presenting an absorption band as a thin film centred at 841 nm (**Fig. 1c**). However, research focusing on the use of pristine Y6 in OFETs/OPTs and the photoresponse of these devices remains notably limited up to the present.

In this work, we investigate the crystallinity of Y6 thin films and assess the optoelectronic response of Y6 OPTs based on BGBC OFETs. Our aim is to study the potential of Y6 as a prospective candidate for NIR OPDs, with potential applications in health monitoring. To this aim, Y6 OFETs will first be fabricated and electrically

characterized in the dark by extracting the figure of merit field-effect mobility (μ_{FE}), which quantifies the ease with which charge carriers flow through the OSC when an electric field is applied, and the threshold voltage (V_{th}), which is the minimum source-gate voltage (V_{SG}) required to switch on the device. Finally, Y6 devices will be studied under NIR illumination and characterized by extracting their photoresponsivity (or responsivity) (R).

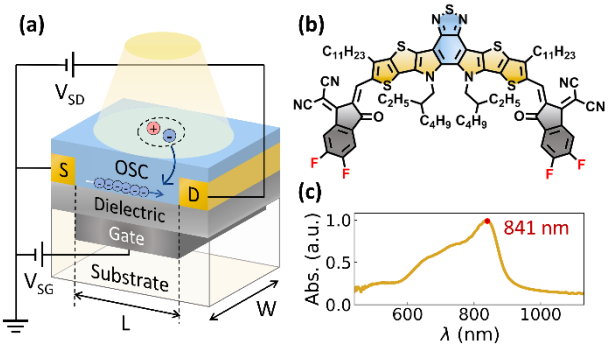

Figure 1. (**a**) OPT with a BGBC OFET architecture. L (length) and W (width) are geometric parameters of the conductive channel. (**b**) Y6 molecular structure (A segments in grey/blue, D segments in yellow), and (**c**) absorption spectrum of Y6 thin film.

2. MATERIALS AND METHODS.

2.1. Fabrication of Y6 OPTs.

To fabricate the Y6 OFETs with a BGBC architecture 500 µm thick silicon wafers (Si/SiO_2) were used, where highly doped silicon (Si p++) acted both as the substrate and gate electrode, and the silicon oxide as the dielectric layer (200 nm thick SiO_2 layer with capacitance $C = 17\ nF/cm^2$ grown on top of the Si p++). The source and drain electrodes were fabricated by means of photolithography and thermal evaporation (5 nm Cr / 40 nm Au). The design used consisted of five interdigitated channels with a length of 200 µm and a total W/L ratio of 100. Regarding the OSC, a solution of Y6 in chloroform (CF) 16 mg/mL was prepared, in which Y6 and CF were left 24 hours stirring at 500 rpm at room temperature. The OSC was deposited on top of the device using the blade coating technique (**Fig. 2a**), which is a low cost thin-film deposition technique that involves running a blade over a substrate at a fixed distance and is compatible with roll-to-roll processing and large-area reparation. First, a meniscus of the Y6 solution was formed between the blade and the sample, which was located on top of a hot plate at 40 ºC. The blade was dragged, forming a thin film of several nanometers thick of the OSC. The sample was left a few minutes on top the hot plate to evaporate most of the solvent. Y6 thin films undergoing thermal annealing were placed in a hot plate at different temperatures for 10 minutes (**Fig. 2b**). All the Y6 thin films were characterized with X-ray diffraction (XRD) and polarized optical microscopy (POM). A scratch on the surface of the wafer was also made using a diamond tip to reach the doped silicon, which acted as the gate electrode.

2.2. Electrical Characterization and Photoresponse Study.

OFET electrical performance was measured on fresh devices using a Keithley 2612A. The two figures of merit of OFETs, the field-effect mobility (μ_{FE}^{sat}) and threshold voltage (V_{th}), were extracted in the saturation regime from a linear fit of the plot $\sqrt{I_{SD}}$ versus V_{SG} using the following relationship:

$$I_{SD}^{sat} = \frac{W}{2L}\mu_{FE}^{sat} C\ (V_{SG} - V_{th})^2 \quad , \qquad (1)$$

where C is the capacitance of the dielectric layer, and L and W are the length and width of the conductive channel respectively. The optical performance of the devices was assessed using a Keithley 2612A and Keithley 2604B equipment and the LED840L light emitting diode (LED) of 840 nm (see **Fig. 2c**), which was previously calibrated. In particular, the dynamic photoresponse was assessed by irradiating the device with light pulses at different intensities. A custom-made setup was created to accurately position the LED over the OFETs for characterization. To quantify the photoresponse, the key figure of merit for OPDs, known as photoresponsivity R, was calculated using equation (2):

$$R = \frac{I_{light} - I_{dark}}{A \cdot P} = \frac{I_{ph}}{A \cdot P} \qquad (2)$$

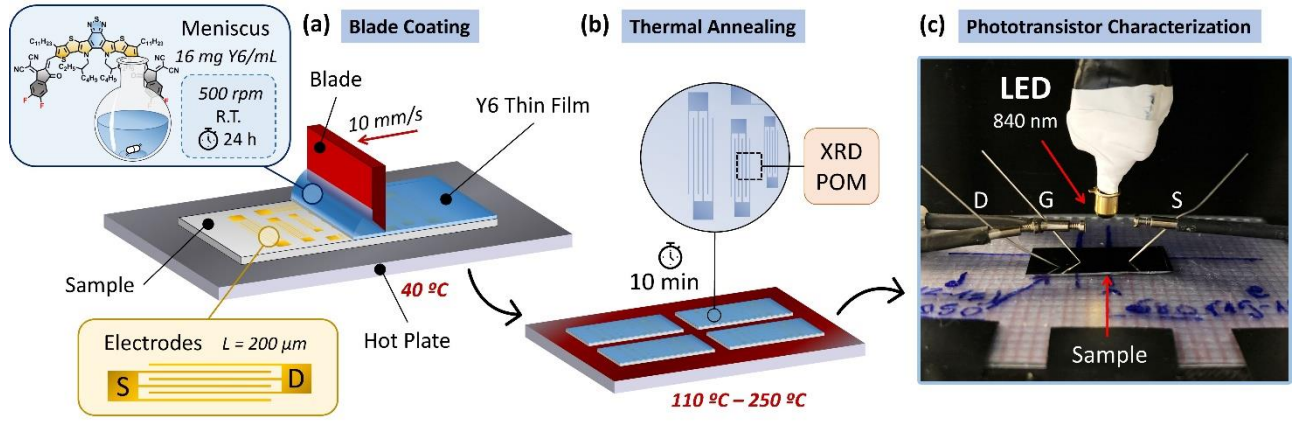

Figure 2. Representation of the experimental procedure.

where $I_{ph} = I_{light} - I_{dark}$ is the photocurrent, A is the

active area of the channel ($A = L \cdot W$) and P is the optical power per unit area.

All the fabrication and characterization processes were performed in a glovebox with inert environment to avoid degradation of the OSC.

3. RESULTS AND DISCUSSION.

3.1. Crystallization of Y6 by Thermal Annealing.

Y6 thin films were thermally annealed at different temperatures, ranging from 110 ºC to 250 ºC. X-ray diffraction (XRD) patterns and polarized optical microscopy (POM) images determined that films annealed at temperatures below 170 ºC presented amorphous characteristics. In contrast, temperatures at or above 170 ºC yielded crystalline films. Higher temperature samples tended to present higher crystalline films with larger mean domain sizes. However, some of the higher temperatures resulted in areas not covered by the organic film due to partial dewetting, which are undesirable as they could compromise device performance.

Therefore, annealing temperatures between 150 ºC and 190 ºC were selected to fabricate and characterize Y6 OFETs with different Y6 thin film morphologies, to understand the relationship between morphology and performance of the devices.

3.2. Electrical Performance of Y6 OFETs.

The μ_{FE}^{sat} and V_{th} parameters were obtained from the transfer measurements of Y6 OFETs subjected at annealing temperatures of 150 ºC, 170 ºC and 190 ºC. **Fig. 3** shows a representative transfer measurement of Y6 OFETs annealed at 170 ºC, where the square root of the source-drain current ($\sqrt{I_{SD}}$) in relation to the source-gate potential (V_{SG}) along with the fit using eq. (1) has also been represented. A summary of the parameters extracted from these transfer characteristics is provided in **Table 1**.

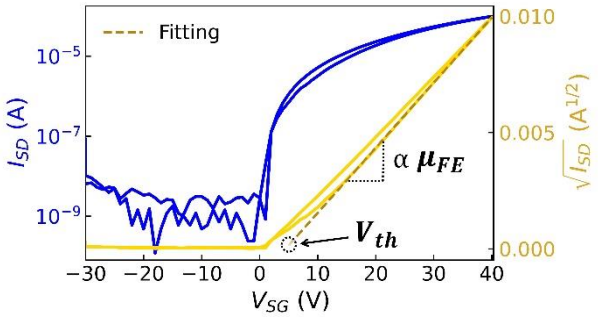

Figure 3. Representative transfer characteristic.

Table 1. Figures of merit of OFETs subjected at different annealing temperatures.

T (ºC)	μ_{FE}^{sat} ($cm^2\ V^{-1}\ s^{-1}$)	V_{th} (V)
150	$(118.8 \pm 9.2) \cdot 10^{-4}$	-3.48 ± 0.47
170	$(9.51 \pm 0.36) \cdot 10^{-2}$	5.2 ± 1.1
190	$(7.61 \pm 0.19) \cdot 10^{-2}$	5.52 ± 0.29

Y6 OFETs annealed at 170-190 ºC present significantly higher mobility values with respect to devices at 150 ºC. which can be attributed to the strong dependence of the transport mechanism on the ordering degree of the OSC thin film. A mobility value of approximately 0.1 $cm^2\ V^{-1}\ s^{-1}$ has been achieved at 170 ºC, which is relatively high for an n-type OSC. Interestingly, devices at 170 ºC outperformed those at 190 ºC, possibly due to 190 ºC samples exhibiting microstructural defects not detected by the characterization methods used in this work.

The negative V_{th} value at 150 ºC suggests that the OFETs starts to conduct at a negative V_{SG}. This behaviour could be due to doping, among other factors. In contrast, positive V_{th} values for the crystalline devices indicate OFETs are in depletion mode, typical of n-type OSCs.

3.3. Photoresponse of Y6 OFETs.

Fig. 4 shows the transfer characteristics of Y6 OFETs annealed at 170 ºC under various incident optical powers of radiation with λ_{max} = 840 nm.

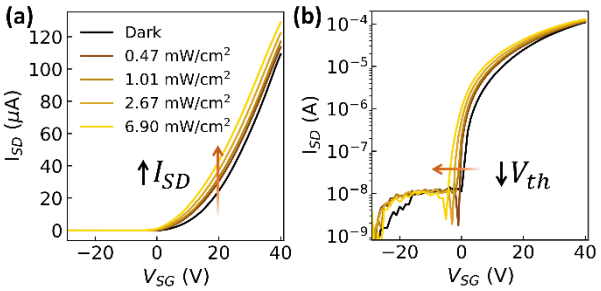

Figure 4. Transfer characteristics under various incident optical powers (**a**) in linear and (**b**) logarithmic scale.

The transfer curves shift to negative threshold voltages and exhibit higher source-drain currents as the incident optical power increases, in comparison to measurements in the absence of light (dark). This is elucidated by the photogenerated excitons within Y6 under light illumination, which, after hole-electron dissociation, produces the generation of additional charges. The fact that Y6 OFET devices respond differently to light than in the dark indicates their potential suitability as OPTs.

Another important parameter of photodetectors is current−time response. **Fig. 5a** displays the dynamic photoresponse of Y6-based OPTs that underwent thermal annealing at 170 ºC with a fixed polarization of $V_{SG} = V_{SD}$ = 10 V under 10-second light pulses (λ_{max} = 840 nm) at varying incident optical powers. The rise time (τ_r) and decay time (τ_{d1}) were determined as the durations needed for the transition from 10% to 90% of the step and from 90% to 10%, respectively (see **Fig. 5b**). These values were found to be approximately 0.3 s and 0.9 s respectively. A second decay time (τ_{d2}) can be obtained by fitting the experimental data to equation (3):

$$I_{SD} = I_{dark} + (I_{light} - I_{dark}) \cdot e^{t_0 - t/\tau_{d2}} \quad (3)$$

where t_0 is the time where measurements begin. By fitting eq. (3) to the dark current after the ON-state, a

mean value of τ_{d2} = (3.01 ± 0.52) s was obtained. These measurements offer valuable insights into the time response of Y6 OPTs, although more precise measurements should be carried out regarding the rise time.

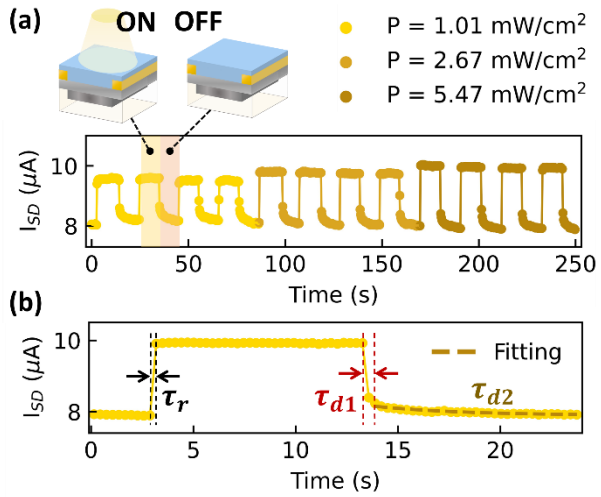

Figure 5. (a) Time measurement with light pulses and **(b)** rise and decay times of Y6 devices.

Finally, photoresponsivity values have been extracted from several measurements at different incident optical powers using eq. (2). **Fig. 6** shows the relationship between both parameters at different polarizations of the Y6 OFETs. It is possible to see that photoresponsivity *R* is not linearly dependent with the incident optical power *P*. Instead, the following relationship has been obtained, given by eq. (4):

$$R = \alpha \cdot P^{\beta - 1} \qquad (4)$$

where α and β are constants. For all polarizations of the Y6 OPTs, β values were smaller than 1, which indicates that the lower the incident optical power, the higher the responsivity in an exponential fashion. This behaviour can be attributed to the distribution of trap states and is advantageous for detecting extremely low intensities. Therefore, Y6 OPTs are more sensitive at lower incident optical powers.

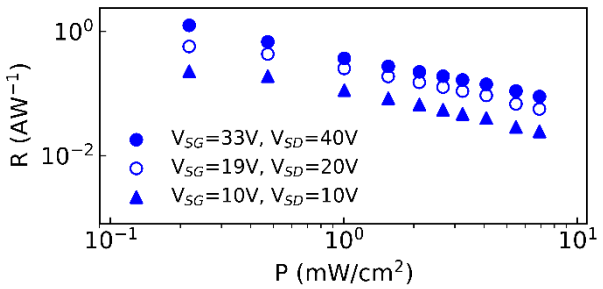

Figure 6. Responsivity versus incident optical power.

4. CONCLUSIONS.

With this work the potential of Y6 as photoactive material in the NIR region has been studied for the first time using OFETs and low-cost fabrication techniques. Our study has shown the importance of thermal annealing in achieving crystallinity of the OSC, which in turn improves the performance of the devices. A high n-type field-effect mobility of approximately 0.1 $cm^2V^{-1}s^{-1}$ has been achieved. Remarkably, it has been demonstrated that Y6 devices can detect NIR light at 840 nm, with higher photoresponsivity values at low incident optical powers. The non-linear relationship found between photoresponsivity and incident power in phototransistors provided insights into their dynamic response. Therefore, this work offers perspectives in the potential of Y6 as a possible candidate for developing NIR OPTs using low-cost fabrication techniques. Future research should focus on adapting Y6 OPTs for flexible substrates and investigating their performance with different incident wavelengths. These efforts would aim to enhance Y6-based phototransistor performance, stability, and versatility for broader optoelectronic applications.

5. REFERENCES.

[1] Li, Qingyuan, Yulong Guo, Yunqi Liu. “Exploration of Near-Infrared Organic Photodetectors”, *Chemistry of Materials* 31.17 (2019): 6359-6379.

[2] García de Arquer, F. Pelayo, et al. “Solution-processed semiconductors for next-generation photodetectors”, *Nature Reviews Materials*, 2.3 (2017): 1-17.

[3] Chen, Y., Wan, X., & Long, G. “High performance photovoltaic applications using solution-processed small molecules”. *Accounts of chemical research*, 46.11, (2013): 2645-2655.

[4] Yuan, Jun, et al., “Single-junction organic solar cell with over 15% efficiency using fused-ring acceptor with electron-deficient core.”, *Joule* 3.4 (2019): 1140-1151.

[5] Gutierrez-Fernandez, Edgar, et al., “Y6 Organic Thin-Film Transistors with Electron Mobilities of 2.4 $cm^2V^{-1}s^{-1}$ via Microstructural Tuning” *Advanced Science* 9.1 (2022): 2104977.